Combining Single Wall Carbon Nanotubes and Photoactive Polymers for Photoconversion

ARTICLE *in* JOURNAL OF THE AMERICAN CHEMICAL SOCIETY · AUGUST 2005

Impact Factor: 12.11 · DOI: 10.1021/ja050396k · Source: PubMed

J|A|C|S
ARTICLES
Published on Web 06/24/2005

Combining Single Wall Carbon Nanotubes and Photoactive Polymers for Photoconversion

G. M. Aminur Rahman,† Dirk M. Guldi,*,‡ Rita Cagnoli,§ Adele Mucci,§ Luisa Schenetti,*,§ Lisa Vaccari,¶ and Maurizio Prato*,¶

Contribution from the Radiation Laboratory, University of Notre Dame, Notre Dame, Indiana 46556, Institute for Physical and Theoretical Chemistry, Egerlandstrasse 3, 91058 Erlangen, Germany, Dipartimento di Chimica, Università di Modena e Reggio Emilia, Via G. Campi 183, 41100 Modena, Italy, and Dipartimento di Scienze Farmaceutiche, Università di Trieste, Piazzale Europa 1, 34127 Trieste, Italy

Received January 20, 2005; E-mail: dirk.guldi@chemie.uni-erlangen.de; schene@unimo.it; prato@units.it

Abstract: A combination of van der Waals and electrostatic interactions was used to integrate **SWNT** and a suitably functionalized polythiophene into nanostructured ITO electrodes. In the resulting electron donor/acceptor nanocomposites, polythiophene represents the light-harvesting chromophore that readily donates an excited-state electron to the ground-state electron-accepting SWNT. Upon illumination, monochromatic incident photoconversion efficiencies between 1.2 and 9.3% were determined for single and eight-sandwiched layers, respectively.

Introduction

Nanoscale carbon-based materials (i.e., fullerenes and carbon nanotubes) represent an attractive platform for optoelectronic and photovoltaic applications.[1−4] The field of electron donor/acceptor interactions has drawn only scattered attention, despite the very intriguing electron-accepting properties of single wall carbon nanotubes (**SWNT**).[5] In particular, the one-dimensional nanowire structure of **SWNT** renders these carbon-based materials ideal for transporting electrons with quasi-ballistic features. **SWNT** possess extended, delocalized π-electron systems, which, in combination with photoexcited electron donors, are expected to be beneficial for testing new paradigms in charge transfer management within novel, ultrahigh efficient photoelectrochemical cells (i.e., nanostructured ITO electrodes).[6]

Linking functional groups to **SWNT** has been an increasingly successful approach toward the controlled decoration of the **SWNT** surface with chromophores, electron donors, biomolecules, etc.[4−6] However, organic functionalization causes dramatic changes on the electronic properties of **SWNT**.[7] For each functionality that is added, an equivalent number of π-electrons are removed from the conjugated π-system. One of the immediate results of the **SWNT** functionalization is the disappearance of the characteristic van Hove singularities in the near-infrared region of the spectrum, which corresponds to the band gap transitions in semiconducting **SWNT**. Consequently, the need for supramolecular means emerges to associate electron donors and **SWNT**, while leaving the π-electronic structure intact. In this context, the simplicity and tunability of van der Waals and electrostatic forces make them particularly interesting.

β-Substituted polythiophenes are organic semiconductors that possess good stability and permit the insertion of functionalities, which allow their processibility in different environments, as

† University of Notre Dame.
‡ Institute for Physical and Theoretical Chemistry.
§ Università di Modena e Reggio Emilia.
¶ Università di Trieste.

(1) (a) *Introduction to Nanotechnology*; Poole, C. P., Owens, F. J., Eds.; Wiley-Interscience: Weinheim, Germany, 2003. (b) *Nanophysics and Nanotechnology: An Introduction to Modern Concepts in Nanoscience*; Wolf, E. L., Ed.; John Wiley & Sons: New York, 2004.
(2) (a) Harris, P. *Carbon Nanotubes and Related Structures: New Materials for the Twenty-First Century*; Cambridge University Press: Cambridge, 2001. (b) *Carbon Nanotubes: Synthesis, Structure, Properties and Applications*; Dresselhaus, M. S., Dresselhaus, G., Avouris, P., Eds.; Springer: Berlin, 2001. (c) Reich, S.; Thomsen, C.; Maultzsch, J. *Carbon Nanotubes: Basic Concepts and Physical Properties*; VCH: Weinheim, Germany, 2004.
(3) Special issue on Carbon Nanotubes. *Acc. Chem. Res.* **2002**, *35*, 997.
(4) For recent reviews, see: (a) Hirsch, A. *Angew. Chem., Int. Ed.* **2002**, *41*, 1853. (b) Bahr, J. L.; Tour, J. M. *J. Mater. Chem.* **2002**, *12*, 1952. (c) Niyogi, S.; Hamon, M. A.; Hu, H.; Zhao, B.; Bhomwik, P.; Sen, R.; Itkis, M. E.; Haddon, R. C. *Acc. Chem. Res.* **2002**, *35*, 1105. (d) Sun, Y.-P.; Fu, K.; Lin, Y.; Huang, W. *Acc. Chem. Res.* **2002**, *35*, 1096. (e) Banerjee, S.; Kahn, M. G. C.; Wang, S. S. *Chem.—Eur. J.* **2003**, *9*, 1898. (f) Tasis, D.; Tagmatarchis, N.; Georgakilas, V.; Prato, M. *Chem.—Eur. J.* **2003**, *9*, 4000. (g) Dyke, C. A.; Tour, J. M. *Chem.—Eur. J.* **2004**, *10*, 812.
(5) (a) Georgakilas, V.; Kordatos, K.; Prato, M.; Guldi, D. M.; Holzinger, M.; Hirsch, A. *J. Am. Chem. Soc.* **2002**, *124*, 760. (b) Murakami, H.; Nomura, T.; Nakashima, N. *Chem. Phys. Lett.* **2003**, *378*, 481. (c) Li, H.; Zhou, B.; Gu, L.; Wang, W.; Shiral Ferando, K. A.; Kumar, S.; Allard, J. F.; Sun, Y.-P. *J. Am. Chem. Soc.* **2004**, *126*, 1014. (d) Guldi, D. M.; Marcaccio, M.; Paolucci, D.; Paolucci, F.; Tagmatarchis, N.; Tasis, D.; Vazquez, E.; Prato, M. *Angew. Chem., Int. Ed.* **2003**, *42*, 4206. (e) Guldi, D. M.; Rahman, G. M. A.; Ramey, J.; Marcaccio, M.; Paolucci, D.; Paolucci, F.; Qin, S.; Ford, W. T.; Balbinot, D.; Jux, N.; Tagmatarchis, N.; Prato, M. *Chem. Commun.* **2004**, 2034. (f) Guldi, D. M.; Rahman, G. M. A.; Tagmatarchis, N.; Prato, M. *Angew. Chem., Int. Ed.* **2004**, *43*, 5526. (g) Rahman, G. M. A.; Guldi, E.; Zambon, E.; Pasquato, L.; Tagmatarchis, N.; Prato, M. *Small* **2005**, *1*, 527. (h) Guldi, D. M.; Taieb, H.; Rahman, G. M. A.; Tagmatarchis, N.; Prato, M. *Adv. Mater.* **2005**, *17*, 871.
(6) (a) Kymakis, E.; Amaratunga, G. A. J. *Sol. Energy Mater. Sol. Cells* **2003**, *80*, 465. (b) Kymakis, E.; Amaratunga, G. A. J. *Appl. Phys. Lett.* **2002**, *80*, 112. (c) Kymakis, E.; Alexandrou, I. *J. Appl. Phys.* **2003**, *93*, 1764. (d) Barazzouk, S.; Hotchandani, S.; Vinodgopal, V.; Kamat, P. V. *J. Phys. Chem. B* **2004**, *108*, 17015. (e) Guldi, D. M.; Rahman, G. M. A.; Jux, N.; Prato, M.; Qin, S.; Ford, W. *Angew. Chem., Int. Ed.* **2005**, *44*, 2015.
(7) (a) Strano, M. S.; Dyke, C. A.; Usrey, M. L.; Barone, P. W.; Allen, M. J.; Shan, H.; Kittrell, C.; Hauge, R. H.; Tour, J. M.; Smalley, R. E. *Science* **2003**, *301*, 1519. (b) Zurek, E.; Autschbach, J. *J. Am. Chem. Soc.* **2004**, *126*, 13079.

Scheme 1 [a]

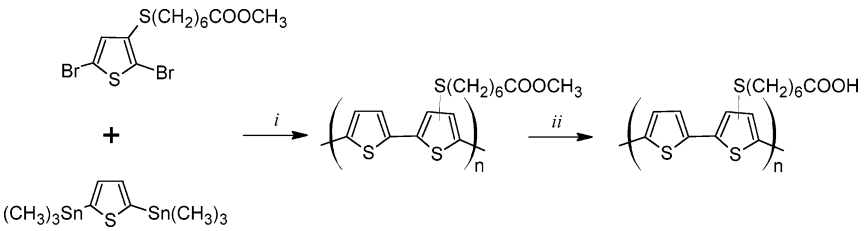

[a] Reagents and conditions: (i) $Pd(PPh_3)_4$, THF/DMF 1:1, 90 °C, 60 h; (ii) NaOH, CH_3OH/THF, 70 °C, 3 h.

well as the tunability of their chemical and physical properties.[8] These materials combine the electroactive properties of the polymeric backbone with those of the side chain groups. Polythiophene-based devices, as modified electrodes or sensors, have been developed for applications both in the gas and in the condensed phase.[9] Studies on poly(alkylsulfanyl)thiophenes have shown that the sulfur atoms, which are directly linked to the thiophene rings, influence some characteristics of these polymers in comparison to polyalkylthiophenes. The oxidation potentials, for example, are appreciably lowered.[10]

Several key aspects prompt to the combination of polythiophenes with **SWNT** for the design of electron donor/acceptor nanocomposites with high photon-to-energy conversion efficiency and high mechanical strength. First, polythiophenes display excellent chromophore features that cover most of the visible range of the solar spectrum.[8] Second, the polythiophenes possess prominent electron donor characteristics, which has led to many practical applications.[10] Third, **SWNT** are good electron acceptors and, at the same time, one-dimensional nanowires. Finally, homogeneous incorporation into polymer matrices has been shown to lead to strong **SWNT** composites.[11] The ultimate tensile strength in such composites was $T = 220 \pm 40$ MPa, with some readings as high as 325 MPa.[12]

To modify photoactive ITO electrodes with multicomponent nanocomposites, which should be thermodynamically stable and robust entities, a fine-tuned interplay of interactions at the nanoscale level is necessary. In this context, the layer-by-layer (LBL) technique brings all the benefits of a powerful methodology.[13] Most eminently, LBL offers great control over (i) the molecularly organized integration of functional building blocks (i.e., **SWNT** and polythiophene) and (ii) the performance of the required function (i.e., solar energy conversion).

Here, we present, for the first time, the supramolecular integration of LBL nanocomposites onto ITO electrodes, comprising polythiophene derivatives that bear carboxylic groups on the alkylsulfanyl side chains and **SWNT**, to which pyrene derivatives are immobilized, en route to versatile donor/acceptor ensembles and the demonstration of monochromatic incident photoconversion efficiencies (IPCE) in the range of 1.2−9.3% for single and eight-sandwich layers, respectively.

Results and Discussion

We generated the copolymer of unsubstituted thiophene and 7-(thien-3-ylsulfanyl)heptanoic acid (**PSCOOH**), hydrolyzing the parent methyl ester, obtained through Stille coupling of 2,5-bis(trimethylstannyl)thiophene and methyl 7-[(2,5-dibromothien-3-yl)sulfanyl]heptanoate (Scheme 1). The presence of the sulfur atom in the side chain is important to improve the donor characteristics of the polymer.[10]

The ^{1}H NMR spectrum of **PSCOOH** (Figure 1) displays the characteristic signal from the carboxylic group at 11.85 ppm and the disappearance of the singlet of CH_3O at 3.64 ppm, confirming the complete hydrolysis of the ester functions. The thiophene signals are centered around 7.34 ppm, SCH_2 and CH_2-COOH protons give the expected signals at 2.99 and 2.16 ppm, respectively. The remaining aliphatic signals are found between 1.6 and 1.1 ppm. The relative content of the two copolymerized units was estimated by the integral ratio between CH_2COOH and aromatic protons, and it was found to be about 2:3, confirming that the utilized comonomer 1:1 feed ratio was maintained. The molecular weight of **PSCOOH** was estimated by gel permeation chromatography (GPC) in THF: weight-average molecular weight, M_w, and number-average molecular weight, M_n, were 3.3×10^3 and 2.1×10^3 g mol^{-1}, respectively, with a polydispersity index, M_w/M_n, of 1.6. For the integration of **PSCOOH** into LBL nanocomposites through electrostatic interactions, the solubility of **PSCOOH** in different polar

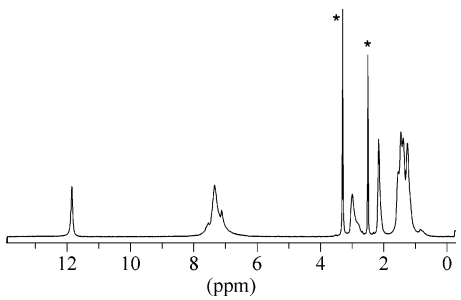

Figure 1. ^{1}H NMR spectrum of **PSCOOH** in DMSO-d_6. Asterisks denote solvent and water signals.

(8) Skotheim, T. A.; Elsenbaumer, R. L.; Reynolds, J. R. *Handbook of Conducting Polymers*; Marcel Dekker: New York, 1998.
(9) Fichou, D. *Handbook of Oligo- and Polythiophenes*; Wiley-VCH: Weinheim, Germany, 1999.
(10) (a) Iarossi, D.; Mucci, A.; Parenti, F.; Schenetti, L.; Seeber, R.; Zanardi, C.; Forni, A.; Tonelli, M. *Chem.—Eur. J.* **2001**, *7*, 676. (b) Iarossi, D.; Mucci, A.; Schenetti, L.; Seeber, R.; Goldoni, F.; Affronte, M.; Nava, F. *Macromolecules* **1999**, *32*, 1390.
(11) (a) Yu, M. F.; Lourie, O.; Dyer, M. J.; Moloni, K.; Kelly, T. F.; Ruoff, R. S. *Science* **2000**, *287*, 637. (b) Wong, E. W.; Sheehan, S. E.; Lieber, C. M. *Science* **1997**, *277*, 1971. (c) Smith, B. L.; Schaffer, T. E.; Viani, M.; Thompson, J. B.; Frederick, N. A.; Kindt, J.; Belcher, A.; Stucky, G. D.; Morse, D. E.; Hansma, P. K. *Nature* **1999**, *399*, 761. (d) Popov, V. N.; Van Doren, V. E.; Balkanski, M. *Phys. Rev. B* **2000**, *61*, 3078. (e) Qian, D.; Dickey, E. C.; Andrews, R.; Rantell, T. *Appl. Phys. Lett.* **2000**, *76*, 2868. (f) Chen, J.; Rao, A. M.; Lyuksyutov, S.; Itkis, M. E.; Hamon, M. A.; Hu, H.; Cohn, R. W.; Eklund, P. C.; Colbert, D. T.; Smalley, R. E.; Haddon, R. C. *J. Phys. Chem. B* **2001**, *105*, 2525.
(12) Mamedov, A. A.; Kotov, N. A.; Prato, M.; Guldi, D. M.; Wicksted, J. P.; Hirsch, A. *Nat. Mater.* **2002**, *1*, 190.
(13) (a) Decher, G.; Hong, J. D. *Ber. Bunsen-Ges. Phys. Chem.* **1991**, *95*, 1430. (b) Ferreira, M.; Cheung, J. H.; Rubner, M. F. *Thin Solid Films* **1994**, *244*, 806. (c) Keller, S. W.; Kim, H. N.; Mallouk, T. E. *J. Am. Chem. Soc.* **1994**, *116*, 8817. (d) Lvov, Y.; Decher, G.; Haas, H.; Mohwald, H.; Kalachev, A. *Physica B* **1994**, *198*, 89. (e) Kotov, N. A. *Nanostruct. Mater.* **1999**, *12*, 789. (f) Dubas, S. T.; Schlenoff, J. B. *Macromolecules* **1999**, *32*, 8153. (g) Hammond, P. T. *Curr. Opin. Colloid Interface Sci.* **2000**, *4*, 430. (h) Durstock, M. F.; Taylor, B.; Spry, R. J.; Chiang, L.; Reulbach, S.; Heitfeld, K.; Baur, J. W. *Synth. Met.* **2001**, 116. (i) Ferreira, M.; Rubner, M. F.; Hsieh, B. R. *MRS Symp. Proc.* **1994**, *328*, 119. (j) Yoo, S.; Shiratori, S. S.; Rubner, M. F. *Macromolecules* **1998**, *31*, 4309.

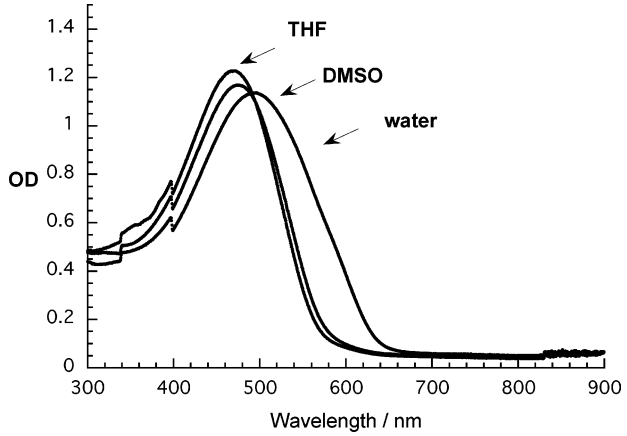

Figure 2. Absorption spectra of **PSCOOH** in different solvents; see label for assignment.

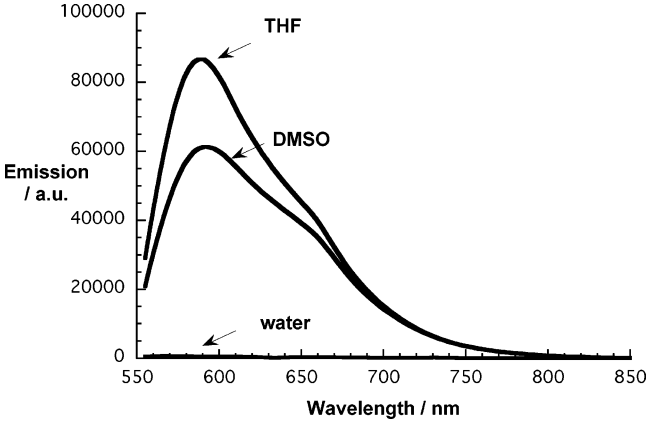

Figure 3. Emission spectra of **PSCOOH** in different solvents with identical absorption at the 500 nm excitation wavelength (i.e., OD = 0.5); see label for assignment.

solvents, such as DMSO, THF, DMF, and aqueous ammonia, due to the presence of the hydrophilic side functionalities, is of vital importance.

To test the most suitable environmental conditions for processing **PSCOOH** (see below), we compared absorption (i.e., Figure 2) and emission features (i.e., Figure 3) in some of the aforementioned solvents. As far as absorption spectra are concerned, we see continuing red-shifts when going from THF to DMSO and water. This is reasonably rationalized when considering the character of the underlying transition, namely, a $\pi-\pi$ transition, which is expected to red-shift. Implicit is that the carbonyl functionality does not mix with and/or dominate the $\pi-\pi$-centered transition.[14] An additional broadening is also discernible, which is a first hint toward aggregation phenomena. Decisive evidence for **PSCOOH** aggregation came from fluorescence experiments. As can be seen from these experiments, the emission is effectively quenched in alkaline media and to a lesser extent in DMSO. Only the use of THF as solvent leads to the expected strong emission. In fact, the high fluorescence quantum yield of 0.15 resembles that found for polythiophene.[15] This suggested to carry out the construction of nanostructured photoelectrodes with **PSCOOH** in THF solutions.

To process **SWNT**, we used noncovalent linking with amphiphilic pyrene derivatives through $\pi-\pi$ interactions. Recently, we have reported that a pyrene derivative, namely, 1-(trimethylammonium acetyl) pyrene (**pyrene**$^+$), forms stable **SWNT·pyrene**$^+$ suspensions, due to the positively charged ammonium headgroup.[5f,16] Typically, these aqueous suspensions contain about 1.6 mg of SWNT in 8 mL of water (see Experimental Section) and are stable for weeks (i.e., see Figure S1 in the Supporting Information). A careful preparation allows the immobilization of more than 80% of **pyrene**$^+$ to the **SWNT** surface, based on the fluorescence quenching. These facts render **SWNT·pyrene**$^+$ most suitable for our strategy to modify ITO electrodes (vide infra).

For the construction of novel, nanostructured photoelectrodes, we capitalized on our previous experience with electrostatically driven LBL deposition techniques.[17] Quartz slides, indium tin oxide electrodes, and silicon wafers were used as substrates to conduct optical characterization, photocurrent measurements, and AFM imaging, respectively. Prior to their use, all substrates underwent a pretreatment procedure. In particular, the hydrophobic nature of the surfaces (i.e., refluxing in 2-propanol) required a baselayer coverage of poly(diallyldimethylammonium), PDDA. Once this initial step was completed, we brought in a layer of poly(sodium-4-styrenesulfonato), PSS, bearing sulfonic acid functionalities onto the positively charged baselayer surface. Alternatively, PSS was directly deposited onto the substrate surface.

Now that the surface is sufficiently overlaid with either a PDDA/PSS template or a PSS template, the **SWNT·pyrene**$^+$ target was deposited by immersing the substrates into aqueous suspensions of **SWNT·pyrene**$^+$.[18] Key to the deposition is the electrostatic interaction between the negatively and positively charged headgroups in PSS (i.e., sulfonate) and **pyrene**$^+$ (i.e., trimethylammonium), respectively. In the final step, **PSCOOH** was grafted to **pyrene**$^+$ of the **SWNT·pyrene**$^+$ layer. At the end of the sequence, PDDA/PSS/**SWNT·pyrene**$^+$/**PSCOOH** and PSS/**SWNT·pyrene**$^+$/**PSCOOH** nanocomposites were constructed onto solid substrates. In parallel, the construction of PDDA/**PSCOOH**/**SWNT·pyrene**$^+$ was pursued to revert the deposition sequence and to test the photocurrent flow.

Evidence for the deposition came from absorption spectra, taken after each deposition increment; this is exemplified for a quartz slide in Figure 4. The strong and broad transitions of the **PSCOOH** chromophore are distinguishable in the visible part of the solar spectrum, while the NIR part is largely governed by weaker transitions associated with **SWNT**. Comparable features evolve for **PSCOOH**/**SWNT·pyrene**$^+$, obtained by inverting the deposition order of the two components. Solution spectra of the individual components, namely, **PSCOOH** and **SWNT·pyrene**$^+$, give rise to similar maxima in THF and water,

(14) Turro, N. *Modern Molecular Photochemistry*; University Science Books: New York, 1991.
(15) Wasserberg, D.; Marsal, P.; Meskers, S. C. J.; Janssen, R. A. J.; Beljonne, D. *J. Phys. Chem. B* **2005**, *109*, 4410 and references therein.
(16) (a) Nakashima, N.; Tomonari, Y.; Murakami, H. *Chem. Lett*. **2002**, 638. (b) Artyukhin, A. B.; Bakajin, O.; Stroeve, P.; Noy, A. *Langmuir* **2004**, *20*, 1442.
(17) (a) Luo, C.; Guldi, D. M.; Maggini, M.; Menna, E.; Mondini, S.; Kotov, N. A.; Prato, M. *Angew. Chem., Int. Ed.* **2000**, *39*, 3905. (b) Guldi, D. M.; Luo, C.; Koktysh, D.; Kotov, N. A.; Da Ros, T.; Bosi, S.; Prato M. *Nano Lett.* **2002**, *2*, 775. (c) Guldi, D. M.; Pellarini, F.; Prato, M.; Granito, C.; Troisi, L. *Nano Lett.* **2002**, *2*, 965. (d) Guldi, D. M.; Zilbermann, I.; Lin, A.; Braun, M.; Hirsch, A. *Chem. Commun.* **2004**, 96. (e) Guldi, D. M.; Kotov, N. A.; Hirsch, A.; Prato, M. *J. Phys. Chem. B* **2004**, *108*, 8770.
(18) For a similar deposition approach of multiwall carbon nanotubes that carry positively charged ionic groups, see: Lou, X.; Detembleur, C.; Pagnoulle, C.; Jerome, R.; Bocharova, V.; Kiriy, A.; Stamm, M. *Adv. Mater*. **2004**, *16*, 2123.

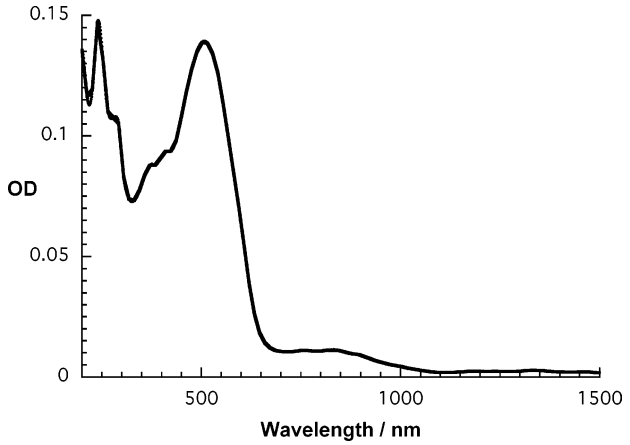

Figure 4. Absorption spectrum of a single **SWNT·pyrene**$^+$**/PSCOOH** sandwich layer on quartz.

respectively. Despite the qualitative resemblance, an overall broadening of the spectrum was observed in the films, which extends out to 1500 nm. Under the current conditions, the broadening reflects the interactions occurring between the individual components (i.e., PDDA, PSS, **SWNT·pyrene**$^+$, and **PSCOOH**) and light scattering in the densely packed films.

Atomic force microscopy measurements (AFM) on silicon wafers complemented our analysis of the deposition sequence. The upper image of Figure 5 demonstrates that the surface becomes almost uniformly covered with characteristic **SWNT** of micrometer dimensions. Relative to the weak NIR absorption shown in Figure 4, the dense coverage can be understood on the basis of weak extinction coefficients of **SWNT·pyrene**$^+$ (i.e., $\sim$10 L g^{-1} cm^{-1}) and the high extinction coefficients of **PSCOOH**.[19] Analyzing the AFM images confirms that, in some cases, the **SWNT·pyrene**$^+$ nanocomposites are constituted of individual **SWNT** rather than consisting of large aggregated bundles. After addition of **PSCOOH**, the typical shape of **SWNT·pyrene**$^+$ is still evident. Inspecting the height of the image shown in Figure 5b, an increased smoothness is deduced, without, however, achieving atomic resolution of **PSCOOH**. Complementary to the AFM investigation, scanning electron micrographs (SEM) were taken (see Figure S2 of the Supporting Information). SEM images qualitatively confirm the presence of carbon nanotubes in **SWNT·pyrene**$^+$ and **SWNT·pyrene**$^+$/**PSCOOH**.

Photocurrents of the modified ITO electrodes were measured under deoxygenated conditions with 1 mM ascorbate/0.1 M Na_3PO_4 solutions. The major UV−vis absorber in the **SWNT·pyrene**$^+$**/PSCOOH** and **PSCOOH/SWNT·pyrene**$^+$ mixed nanocomposites is **PSCOOH**. PDDA, PSS, and **SWNT·pyrene**$^+$ are relatively weak absorbers in the region of interest, that is, between 350 nm and the NIR. Thus, not surprisingly, the photoaction spectra of ITO electrodes modified with **SWNT·pyrene**$^+$**/PSCOOH** and **PSCOOH/SWNT·pyrene**$^+$, as illustrated in Figure 6, track the spectral features that the **PSCOOHs** exhibit in solution and deposited on quartz (compare Figure 6 with Figures 2 and 4).[20]

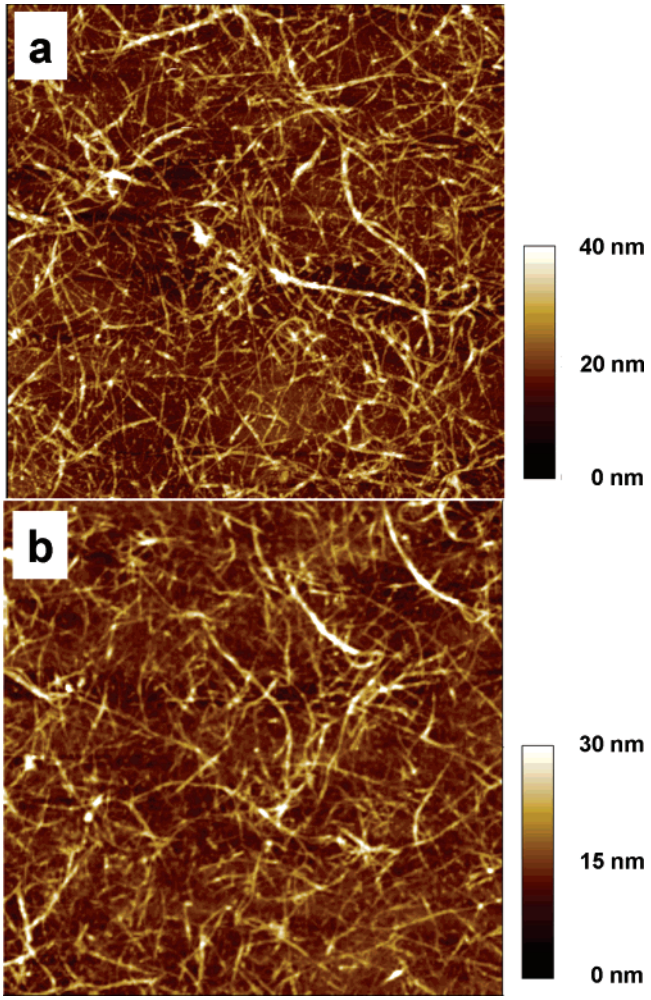

Figure 5. AFM images of (a) a **SWNT·pyrene**$^+$ and (b) a single **SWNT·pyrene**$^+$**/PSCOOH** sandwich layer on silicon wafers; image size is 5 μm $\times$ 5 μm.

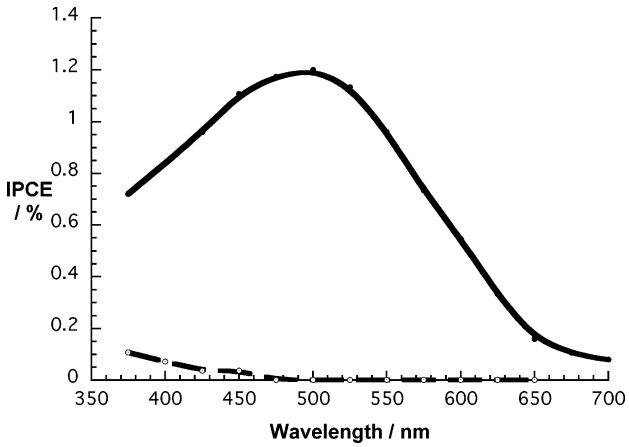

Figure 6. Photoaction spectrum of **SWNT·pyrene**$^+$ (dashed line) and a single **SWNT·pyrene**$^+$**/PSCOOH** (solid line) sandwich layer: 0.1 M Na_3PO_4, 1 mM sodium ascorbate, no electrochemical bias.

Prior to mechanistic investigations, the photocurrents were tested as a function of incident photon flux. For most of the correlation (i.e., 200−500 W) shown in Figure S3, a linear dependence was noted, which led us to use 400 W in our experimental work. By converting the photocurrents into monochromatic device efficiencies, anaerobic IPCE values of 0.1 and 1.2% were estimated for **SWNT·pyrene**$^+$ and **SWNT·**

(19) Paloniemi, H.; Aaritalo, T.; Laiho, T.; Liuke, H.; Kocharova, N.; Haapakka, K.; Terzi, F.; Seeber, R.; Lukkari, J. *J. Phys. Chem. B* **2005**, ASAP.
(20) In the absence of the visible light-harvesting **PSCOOH**, the photocurrent generation of just **SWNT/pyrene**$^+$ responds mainly to the light >400 nm, similar to the observation in ref 6d; see Figure 6.

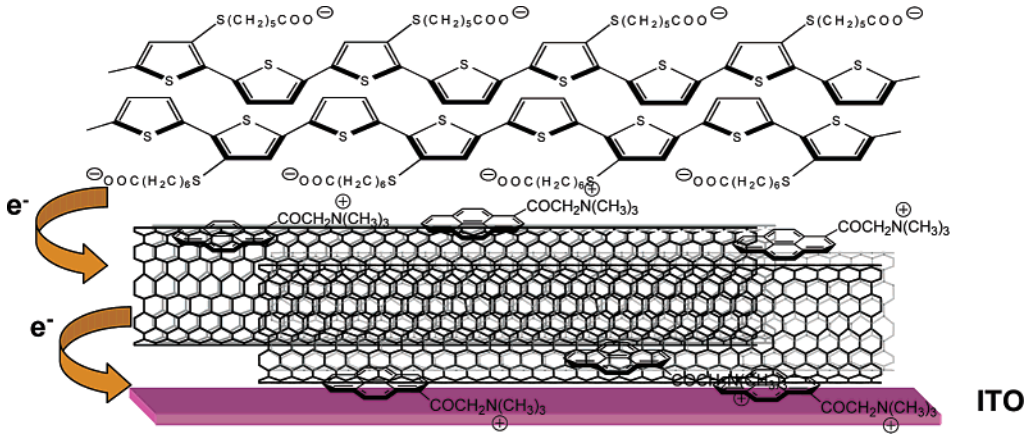

Figure 7. Schematic representation of electron transfer events in modified ITO electrodes bearing a single **SWNT·pyrene$^+$/PSCOOH** sandwich layer; baselayers of PDDA and PSS are omitted from the sketch.

pyrene$^+$/PSCOOH at their peak intensities at 375 and 500 nm, respectively.[21] Relative to a bare ITO electrode that is covered with the polyelectrolyte and that gives rise to 0.001%, this is a significant improvement.[22] Replacing **SWNT·pyrene$^+$** with **C_{60}^-** (i.e., dendritic C_{60} oligocarboxylate)—as the electron acceptor unit—gave an IPCE value of 0.01%.[22] Barely higher (i.e., 0.02%) were the IPCEs for a **C_{60}^+** (i.e., *trans*-2-bispyrrolidinium salt)/**PSCOOH** cell.[23] It is likely that the fullerene (i.e., **C_{60}^-** or **C_{60}^+**) may act as a blocking layer in these cells.

In **PSCOOH** reference cells, namely, the ITO electrode covered with a **PSCOOH** layer, an IPCE of 0.75% was estimated. More significant is the observation that adding **SWNT·pyrene$^+$** does, in the corresponding **PSCOOH/SWNT·pyrene$^+$** cell, not impact at all the photocurrent (i.e., 0.75%).

For the photocurrent generation, a mechanistic picture evolves, which is sketched in Figure 7. An important factor is that our LBL deposition places the electron acceptor (i.e., **SWNT·pyrene$^+$**) in close position relative to the ITO electrode, while the electron donor/chromophore (i.e., **PSCOOH**) is located at the aqueous interface. Upon the initial photoexcitation of **PSCOOH**, a thermodynamically driven electron transfer occurs to oxidize **PSCOOH** and to reduce **SWNT**. Electron injection from the reduced **SWNT** into the conduction band of ITO (i.e., −0.25 V versus SCE)[24] and sacrificial electron transfer from ascorbate to the oxidized **PSCOOH** reinstate the ground state of **SWNT·pyrene$^+$/PSCOOH**. Independent confirmation for this hypothesis is based on electrochemical biasing the ITO electrode. With increasingly negative potentials, the photocurrents drop, while an opposite trend is observed in the positive region. Changing, for example, the electrochemical bias from −200 to +200 mV, which does not impact any of the electroactive components (i.e., **SWNT**, **pyrene$^+$**, **PSCOOH**, ascorbate), leads to a 5-fold photocurrent amplification.

A contrasting trend is noted for **PSCOOH/SWNT·pyrene$^+$**. Initial charge separation within **PSCOOH/SWNT·pyrene$^+$** is followed by hole injection into the ITO electrode. Applying a negative bias at the ITO electrode surface is expected to facilitate the hole injection from the oxidized electron donor (i.e., **PSCOOH**). In fact, changing the bias from +200 to 0 mV and to −200 mV versus Ag/AgCl leads to a 1.5 and 1.8 increase of the photocurrent, respectively.

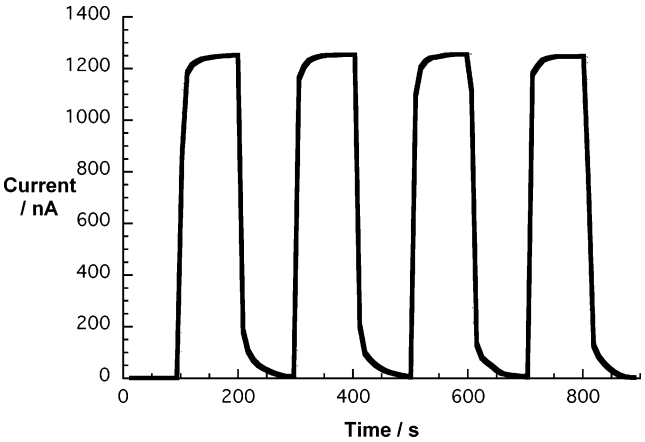

Figure 8. On/Off cycles for a single **SWNT·pyrene$^+$/PSCOOH** sandwich layer: 0.1 M Na_3PO_4, 1 mM sodium ascorbate, no electrochemical bias.

Independent confirmation for these assignments came from adding an electron acceptor (molecular oxygen). In the absence of ascorbate, the addition of oxygen results in a concentration-dependent loss in photocurrent efficiency for **SWNT·pyrene$^+$/PSCOOH**, up to around 25% loss. A competition between **SWNT·pyrene$^+$** and O_2 in deactivating **PSCOOH** excited states is likely to be responsible for this trend. On the contrary, for the **PSCOOH/SWNT·pyrene$^+$** cell, the presence of molecular oxygen leads to small increases in photocurrent. We assume that when O_2 interacts with **SWNT·pyrene$^+$**, a charge shift occurs from **SWNT** to O_2, which subsequently transports the charge to ITO, enhancing thereby the photocurrent generation.

To probe the stability of the photocurrents, nanostructured ITO electrodes were illuminated over several time intervals. A typical example is shown in Figure 8. Only a $CuSO_4$ filter was employed to cut off the wavelength region that would correspond to the illumination of the ITO electrode itself. Importantly, the response to On/Off cycling (i.e., turning the light source on and off) is prompt and reproducible. Over the monitored time window, a moderate change in current of less than 5% was noted.

Sequential repetition of the **SWNT·pyrene$^+$** and **PSCOOH** deposition enabled the systematic stacking of (**SWNT·pyrene$^+$/PSCOOH**)$_n$ sandwich stacks. Again, absorption spectroscopy was used to monitor the regularities of the stepwise deposition

(21) In the case of employing just PSS baselayers, instead of PDDA/PSS, photocurrent efficiencies drop by ca. 15%.
(22) Guldi, D. M.; Zilbermann, I.; Anderson, G. A.; Li, A.; Balbinot, D.; Jux, N.; Hatzimarinaki, M.; Hirsch, A.; Prato, M. *Chem. Commun.* **2004**, 726.
(23) Unpublished results.
(24) Fromherz, F.; Arden, W. *J. Am. Chem. Soc.* **1980**, *102*, 6211.

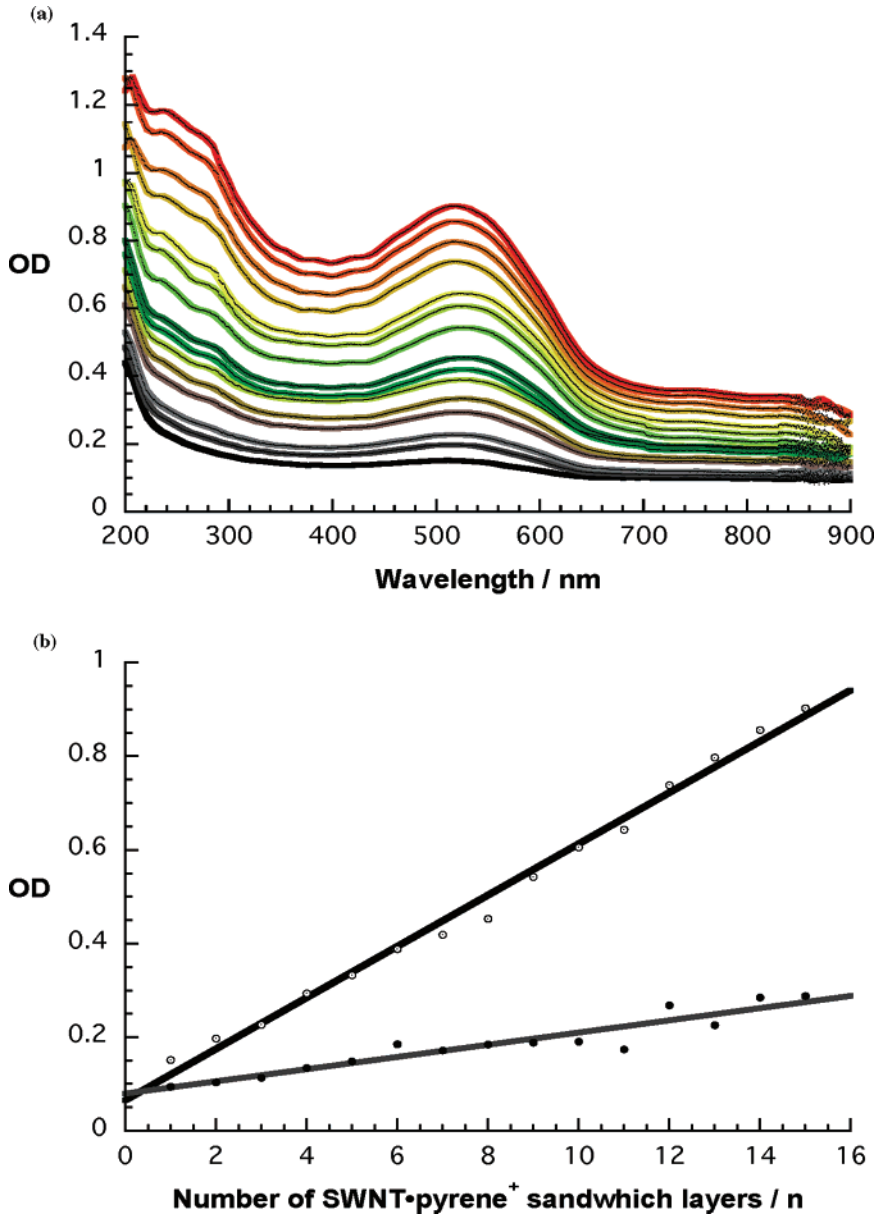

Figure 9. (a) Absorption spectra of variable (i.e., up to 15) (**SWNT·pyrene**$^+$/**PSCOOH**)$_n$ sandwich layers on quartz. (b) Dependence of absorption at 900 (open circles) and 510 nm (circles) as a function of (**SWNT·pyrene**$^+$/**PSCOOH**)$_n$ sandwich layers reflecting the linear growth of **SWNT·pyrene**$^+$ and **PSCOOH**, respectively.

procedure. From the absorption spectra of the deposited films on quartz (Figure 9a), repeatable absorption patterns were deduced. Please note that we reach remarkably strong absorbing surfaces, with absorbances in the visible region of up to 1. The underlying linear dependences at 900 and 510 nm (Figure 9b) are meaningful criteria that confirm the satisfactory and uniform stacking of sequentially deposited **SWNT·pyrene**$^+$ and **PSCOOH** layers.

Interestingly, the steady-state photocurrents (i.e., recorded approximately 10 s upon light exposure) increased notably with increasing (**SWNT·pyrene**$^+$/**PSCOOH**)$_n$ sandwich layers (see Figure 10). This observation can be rationalized on the grounds of higher absorption cross-sections at higher coverage. However, the noted photocurrent amplification is only possible through profitable interactions at the **SWNT·pyrene**$^+$/**PSCOOH** interface, through favorable charge transport features across the sandwich layers and good electronic coupling of any given layer

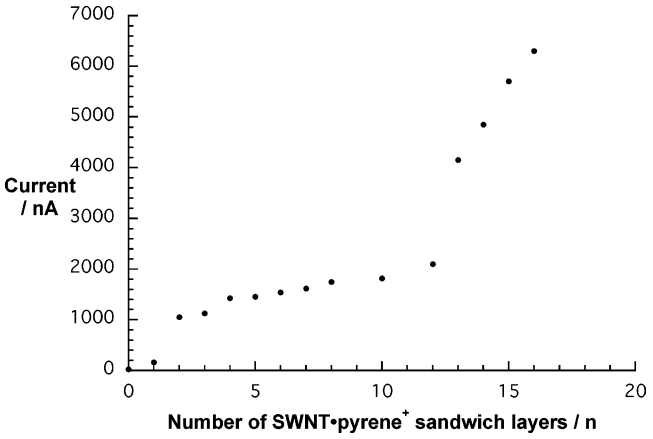

Figure 10. Photocurrent dependence for (**SWNT·pyrene**$^+$/**PSCOOH**)$_n$ sandwich layers.

with the electrode surface. After transforming the photocurrents into monochromatic IPCE, we obtained maximum values as high as 9.3%.

Conclusions

In summary, van der Waals and electrostatic interactions were used to integrate single wall carbon nanotubes (i.e., **SWNT·pyrene**$^+$) and polythiophene (i.e., **PSCOOH**) into photoactive ITO electrodes. Most importantly, monochromatic incident photoconversion efficiencies (IPCE) of 1.2 and 9.3% were determined for single and eight-sandwiched layers, respectively. Such simple organization principles provide the means for an evident trend toward the facile preparation of materials of high current interest.

Experimental Section

Preparation of SWNT·pyrene$^+$. Water-soluble **SWNTs** were obtained in analogy to previous work, using 1-(trimethylammonium acetyl)pyrene (**pyrene**$^+$).[16] In detail, 2 mg of SWNT was dispersed in 8 mL of H_2O that contained 10 mg of **pyrene**$^+$. The mixture was briefly sonicated, after which it was centrifuged. The solid, consisting of 4 mg, was taken out, and the solution was carried on. However, to reduce the amount of free pyrene in solution, the **SWNT**/**pyrene**$^+$ complex was separated through ultracentrifugation (i.e., 10000 r/min for 30 min), and the recovered solid was resolubilized in water.

Film Preparation. A 1% solution of PDDA (pH = 8.5) and DI water for rinsing (pH = 7.2) were used. All solutions were made in deionized water/phosphate buffer. Wafers/ITO/quartz slides were cleaned in piranha solution, rinsed with deionized water, sonicated for 15 min, and again thoroughly rinsed with deionized water. After that, they were coated with a precursor layer of PDDA and/or PSS (10 min exposure), followed by deposition of **SWNT·pyrene**$^+$ and **PSCOOH** (60 min exposure).

Photoelectrochemical Measurements. Photoelectrochemical measurements were carried out in a 3-arm cell that had provision to insert a working electrode (ITO), counter (Pt gauze) and reference (Ag/AgCl) (when bias voltage was applied). The electrolyte was either 0.1 M Na_3PO_4 and N_2, or O_2 was bubbled into the solution for 10−15 min prior to photoelectrochemical measurements. The voltage was applied using a Princeton Applied Research, model 175 galvanostat/potentiostat. Photocurrent measurements were carried out using a Keithley 6485 picoammeter immediately after illumination. A collimated light beam from a 1000 W xenon lamp was used for UV illumination. When white light was used, a 375 nm cut filter was used. When recording a photoaction spectrum, a Bausch and Lomb high-intensity grating monochromator was introduced into the path of the excitation beam for selecting the required wavelengths. All measurements were done after subtracting the stable dark current. The incident photon to current conversion efficiency (IPCE), defined as the number of electrons collected per incident photon, was evaluated from short circuit photocurrent measurements at different wavelengths versus the photocurrent measured using a photodiode of the type PIN UV 100 (UDT Sensors Inc.).

Synthesis of PSCOOH. ^{1}H NMR measurements were performed with a Bruker Avance400 spectrometer operating at 400.13 MHz. Gel permeation chromatography (GPC) was carried out using an Hewlett-Packard system equipped with a Plgel column and a diode array UV detector, with THF as the eluant (1 mL min^{-1}), at room temperature. The average molecular weights were calculated using a calibration curve of monodisperse polystyrene standards.

Copolymerization of 7-[(2,5-Dibromothien-3-yl)sulfanyl]heptanoate and 2,5-Bis(trimethylstannyl)thiophene. In a screw-capped Schlenk tube equipped with a perforable septum, a solution of methyl 7-[(2,5-dibromothien-3-yl)sulfanyl]heptanoate (0.578 g, 1.39 mmol) and 2,5-bis(trimethylstannyl)thiophene (0.730 g, 1.78 mmol) in 3 mL of anhydrous THF/DMF (1:1) was added dropwise to 19.0 mg (0.017 mmol) of $Pd(PPh_3)_4$ in 3 mL of anhydrous THF/DMF (1:1) under argon. The mixture was stirred at 90 °C for 60 h and concentrated to small volume, then CH_3OH (5 mL) was added. The red precipitate was filtered and extracted in Soxhlet with CH_3OH (14 h), *n*-pentane (10 h), and $CHCl_3$ (14 h). $CHCl_3$ was removed under vacuum, giving 0.200 g (42% yield) of poly[(methyl 7-(3-thienylsulfanyl)heptanoate-*co*-thiophene] as a dark-reddish film. ^{1}H NMR (400 MHz, $CDCl_3$, Me_4Si): δ 7.07 (bs, 3H, thiophene), 3.64 (s, 3H, OCH_3), 2.89 (bs, 2H, SCH_2), 2.28 (bs, 2H, CH_2CO), 1.81−1.16 (bs, 8H, 4 CH_2).

Hydrolysis of Poly[methyl 7-(3-thienylsulfanyl)heptanoate]-*co*-thiophene]. To a solution of the polymer (0.200 g) in THF (30 mL) was added methanolic NaOH (10%, 30 mL). The mixture was stirred at 70 °C for 3 h, diluted with water (30 mL); the organic solvent was evaporated under reduced pressure, and 10% aqueous H_2SO_4 was added to adjust pH to 3. The red solid formed was filtered, washed with water, and dried to afford **PSCOOH**-a (0.158 g, 99%) as a dark-reddish powder.

Acknowledgment. This work was carried out with partial support from the EU (RTN network "WONDERFULL"), MIUR (PRIN 2004, prot. 2004035502), SFB 583, and the Office of Basic Energy Sciences of the U.S. Department of Energy. This is document NDRL-4612 from the Notre Dame Radiation Laboratory.

Supporting Information Available: Absorption spectra of **SWNT/pyrene**$^+$ in D_2O, scanning electron micrographs, and photocurrent versus incident photon flux dependence. This material is available free of charge via the Internet at http://pubs.acs.org.

JA050396K